IJARST

International Journal of Advanced Research in Science and Technology

journal homepage: www.ijarst.com

ISSN 2319 – 1783 (Print)
ISSN 2320 – 1126 (Online)

Structural, Electrical and Magnetic Studies on $Cu_{(1-x)}Zn_xFe_2O_4$ Nanoparticles Synthesized by Co-Precipitation method.

D. Santhosh Kumar[1]*, K. Chandra Mouli[2], N. V. Siva Krishna[1] and G. V. Gaurav[3]

[1]Department of Physics, Gayatri Vidya Parishad College for Degree and PG Courses (A), Visakhapatnam-530045, India.

[2]Department of Engineering Physics, AU College of Engineering, Andhra University, Visakhapatnam-530003, India.

[3]Department of Chemistry, Gayatri Vidya Parishad College for Degree and PG Courses (A), Visakhapatnam-530045, India.

****Corresponding Author's Email: drdhavala@gmail.com***

ARTICLEINFO

Article history:
Received : 02 Nov.2019
Accepted : 19 Jan. 2020
Available online : 09 Feb. 2020

Keywords:
Nano particles,
Co-precipitation,
Morphology,
Hysteresis curves,
Soft ferrites.

ABSTRACT

Magnetic Nano particles of $Cu_{(1-x)}Zn_xFe_2O_4$ have been synthesized using Coprecipitation technique. During the experimental investigation, CuZn ferrites exhibited interesting structural, electrical and magnetic properties. Formation of spinel phase was identified using X-Ray diffraction (XRD) technique. The ferrite compounds prepared in the laboratory exhibited cubic spinal symmetry. The Lattice constants of the compounds were determined. The morphology and size of the crystallite was found by Transmission Electron Microscopy (TEM). The magnetic properties were studied using Vibration Sample Magnetometer (VSM) and the saturation magnetization (Ms), remenant magnetization (Mr) and the Coercivity force (Hc) values were evaluated. Electrical properties of the samples were quantified using standard two-probe method.

© 2020 International Journal of Advanced Research in Science and Technology (IJARST). All rights reserved.

PAPER-QR CODE

IJARST

Volume 9, Issue 1

Citation: *Santhosh Kumar et. al. Predictors of Hypocalcemia In Post Thyroidectomy Patients. Int. J. Adv. Res. Sci. Technol. Volume 9, Issue 1, 2020, pp.818-824.*

Introduction:

Ferrites are very important materials in modern technological devices such as microwave absorbers, computer memories, radio and television, satellite communication, digital recording, transformer cores and high quality filters[1,2]. With the recent advent of nanoferrites, microwave technologies have acquired attention for a wide variety of potential applications. Stealth technology is one of such needful for military applications. Ferrites are also have their leap as absorbing material in which copper is the main constituent. In general in literature, copper ferrites have no significance earlier due to their non-applicability for high frequency applications. But copper ferrite nanoparticles are gaining a significant attention among researchers to have much focus on it.

Recently ferrite research has been shifted towards developing these materials in nanometric scales as the performance in their conventional bulk preparation routes in reaching their limits due to their higher electrical conductivity and domain wall resonance [3,4]. However, the technological advances in electronics industry demand even more compact cores for work at higher frequencies[5]. One way to solve this problem is by synthesizing the ferrite particles in nano scale. When the size of the magnetic particles is smaller than the critical size for multi domain formation, the particle exists in a single domain state and domain wall resonance is avoided, thus the material can work at higher frequencies.

There are several methods for synthesizing nano sized spinel ferrite particles. Chemistry-based novel processing routes have been developed in synthesizing ultra fine ferrite powders. Recently, the Sol-gel method[6], co-precipitation method[7], micro wave hydrothermal method[8], citrate gel process[9] and combustion method[10-12] are widely used to prepare different kind of nano scale ferrite particles, such as $ZnFe_2O_4$[13], $Ba(CoTi)_xFe_{12-x}O_{19}$[14]. It is far from clear whether the different routes produce the same microstructures but in the present work reports the results of the powders of the ferrite systems

generated by Co-Precipitation that provides good control over the particle size and produce samples in relatively short times. The aim of the present work is to report and discuss the results of structural, electrical and magnetic properties of $Cu_{(1-x)}Zn_xFe_2O_4$ ferrite nano particles prepared by the co- precipitation method.

Experimental:

In the present work $Cu_{(1-x)}Zn_xFe_2O_4$ nanoparticles were prepared by co- precipitation by taking the high purity starting materials (copper chloride, Zinc chloride and Iron III chloride) as chloride salts as initial ingredients in making the cationic solutions. The co-precipitating, NaOH, made dissolved in measured quantities of deionized water and then added drop by drop to the cationic solution under continuous stirring with a constant speed. The reaction temperature was maintained constant, by manipulating with alkaline aqueous solution. The precipitation occurred immediately and color of suspension changed from grey to dark brown. It was kept stirred for two hours at constant speed, at constant temperature and then precipitate was washed free of chlorides with distilled water. The washed sample was dried in air and the dried sample was examined by X-ray powder diffraction, Transmission Electron Microscope and Vibration Sample Magnetometer. X- Ray powder diffraction was achieved using Cu-Kα source and mean crystallite size was estimated using Debye- Scherer formula applying to the FWHM of the (311) peak of X- Ray diffraction[15]. The particle size and shape of the particles were characterized by Transmission Electron Microscopy (TEM). The magnetization loops for the samples were measured using Vibrating Sample Magnetometer (VSM, JDM-13). Fine powders of $Cu_{(1-x)}Zn_xFe_2O_4$ was mixed with 5% P.V.A binder and pressed into pellets of the size 10mm diameter and thickness range between 2 and 4 mm under a pressure of 50 kN applied for 3 min. these pellets were sintered in air at temperatures 900, 1000, 1100, 1200, 1300^OC respectively, for 2h, by setting heating and cooling rate at 5^OC per minute. The pellets were coated with silver paint on either side in order to establish good ohmic contacts with the electrodes. Resistivity as a function of temperature was measure by using standard two-probe method.

Result and Discussion:

The powder diffraction patterns of copper-zinc ferrites were produced in Fig.1. The spinal peaks corresponding to (200), (311), (400), (422), (511) and (440) planes can be seen clearly confirming the formation of single phase spinal crystal structure. The broadening of the peaks can be attributed to the small size of the particles of polycrystalline powder. $ZnFe_2O_4$ is a cubic spinel and the peak positions in Fig.1 match well with the reported values[16,17]. $CuFe_2O_4$ can have tetragonal as well as cubic lattice, slow cooling leads to stable tetragonal structure[18]. The lattice parameter a (A^o) is calculated for all samples and was listed in Table.1. The XRD patterns of our samples prepared by co-precipitation method match with those reported by others[19,20] confirming the cubic structure and the formation of tetragonal form is ruled out. The XRD pattern of intermediate compounds also matches with the $CuFe_2O_4$ confirming cubic spinal formation. The particle sizes were calculated using Scherer formula and are listed in Table: 1. and they were found to be in the range 15- 21 nm. A gradual increase in the lattice constant is observed with increasing Zn concentration which suggests the formation of solid solution between $CuFe_2O_4$ and $ZnFe_2O_4$, $Cu_{(1-x)}Zn_xFe_2O_4$. The observed increase in a_o with increasing content of zinc in the sample can be ascribed to large ionic radius of Zn^{2+} ions (radius=0.074nm) compared to Cu^{2+} ions (radius= 0.069nm).

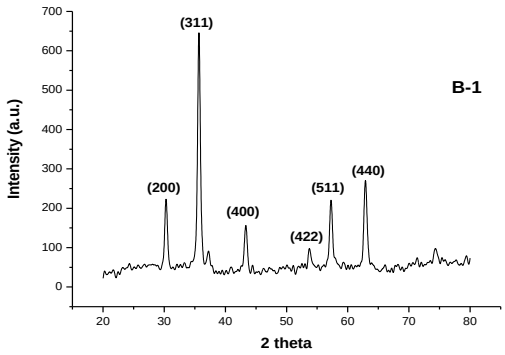

Fig. 1.a: Indexed XRD pattern for $CuFe_2O_4$.

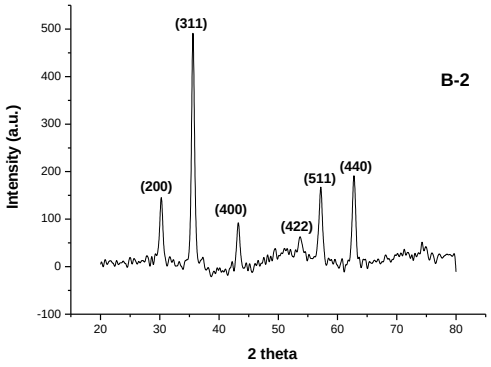

Fig. 1.b: Indexed XRD pattern for $Cu_{0.8}Zn_{0.2}Fe_2O_4$.

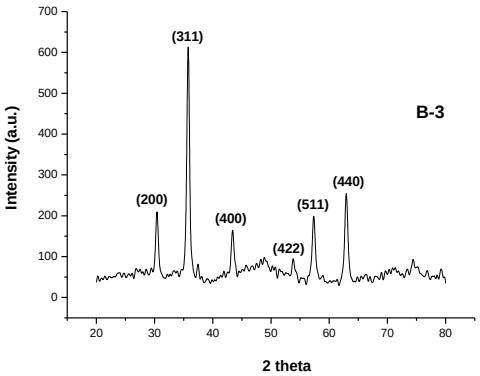

Fig. 1.c: Indexed XRD pattern for $Cu_{0.6}Zn_{0.4}Fe_2O_4$.

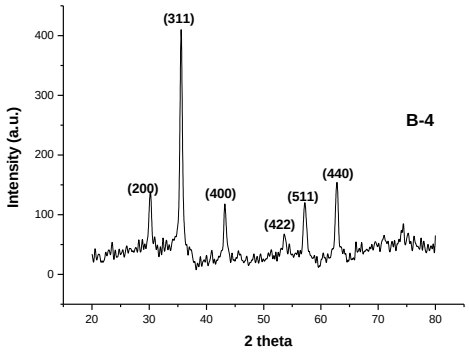

Fig. 1.d: Indexed XRD pattern for $Cu_{0.4}Zn_{0.6}Fe_2O_4$.

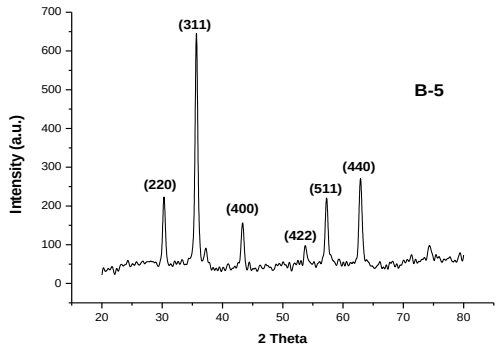

Fig. 1.e: Indexed XRD pattern for $Cu_{0.2}Zn_{0.8}Fe_2O_4$.

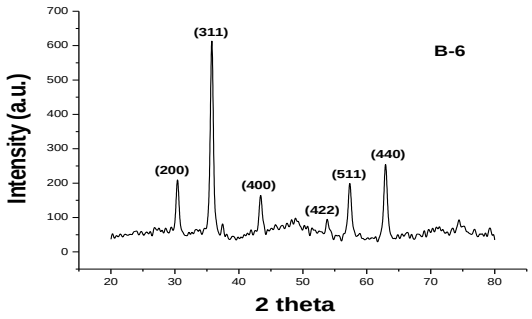

Fig. 1.f: Indexed XRD pattern for $ZnFe_2O_4$.

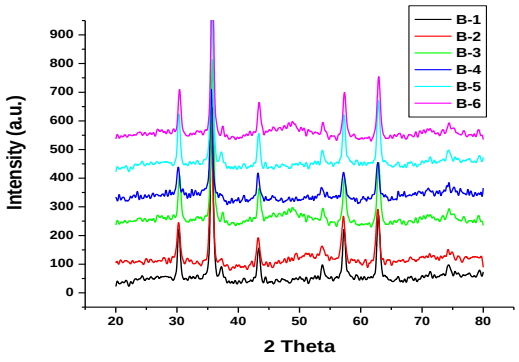

Fig. 2: Indexed XRD pattern for $Cu_{(1-x)}Zn_xFe_2O_4$ with x varying from 0 to1.

Table 1: Particle size and Average lattice Parameter of $Cu_{(1-x)}Zn_xFe_2O_4$.

Sample Name	(hkl)	Particle Size (nm)	a(A^o)
$CuFe_2O_4$	311	16.93	8.3800
$Cu_{0.8}Zn_{0.2}Fe_2O_4$	311	15.49	8.4019
$Cu_{0.6}Zn_{0.4}Fe_2O_4$	311	17.33	8.4103
$Cu_{0.4}Zn_{0.6}Fe_2O_4$	311	20.84	8.4138
$Cu_{0.2}Zn_{0.8}Fe_2O_4$	311	18.78	8.4189
$ZnFe_2O_4$	311	19.45	8.4172

Fig. 2 shows the Transmission Electron Microscopic images of the samples. The images seem to be uniform with cubic shaped particles. The average particle sizes have been estimated to be in the range 15nm to 21nm which is in good agreement with those obtained from X-ray diffraction peaks using Debye-Scherrer formula. The densities of the sintered pellets were measured through Archimedes principle and were given in the Table 2. The density of sintered $Cu_{(1-x)}Zn_xFe_2O_4$ ferrites is found to be increasing with the sintering temperature. The density may be attributed to the existence of phase transition which occurs during the crystal formation process while sintering.

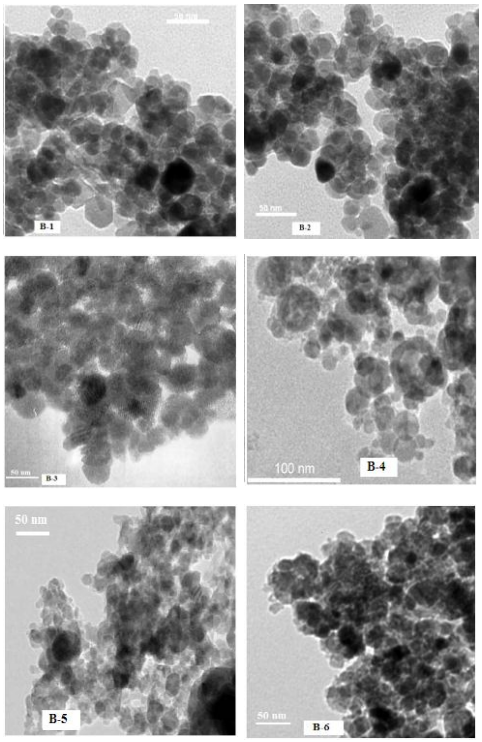

Fig.2. Transmission Electron Micrographs of the prepared samples

The investigation on fine grainy structure of copper-zinc ferrite clearly reveals the uniform development of grains with uniform rate of diffusion. The observed trend in sintered density values reflected in dc resistivity values. Fig.3 to 7 Shows plot of temperature versus log of resistivity for $Cu_{(1-x)}Zn_xFe_2O_4$ ferrite. A semiconductor like general behavior is observed exhibiting straight line nature. Resistivity values at

300K are seem to vary between 3.969 X 10^6 ohm-cm to 4.343 X 10^6 ohm-cm for sample sintered at different temperatures the highest and lowest being observed for 900^0C and 1300^0C respectively.

Table 2: Table showing density of Un-sintered samples and density of samples sintered at 900,1000,1100,1200, and 1300^OC

Name of the Sample	Un Sintered density (g/cc)	900^OC density (g/cc)	1000^OC density (g/cc)	1100^OC density (g/cc)	1200^OC density (g/cc)	1300^OC density (g/cc)
$CuFe_2O_4$	2.6412	3.4261	3.9726	4.1985	4.4651	4.8242
$Cu_{0.8}Zn_{0.2}Fe_2O_4$	2.4986	3.3416	3.8129	4.1019	4.3972	4.7164
$Cu_{0.6}Zn_{0.4}Fe_2O_4$	2.3819	3.4731	3.7826	4.1642	4.4762	4.7219
$Cu_{0.4}Zn_{0.6}Fe_2O_4$	2.3028	3.5982	3.8619	4.2019	4.4973	4.7826
$Cu_{0.2}Zn_{0.8}Fe_2O_4$	2.4897	3.6179	3.9243	4.3269	4.5078	4.8153
$ZnFe_2O_4$	2.7143	3.6412	3.9917	4.4613	4.5173	4.8347

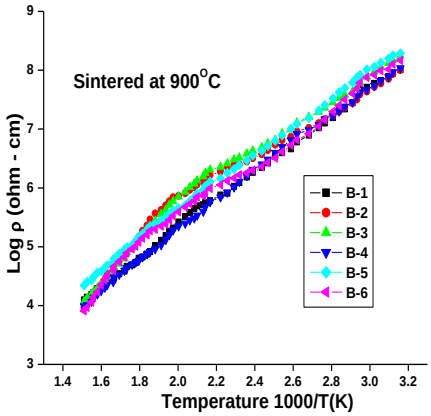

Fig. 3: Plots of Log ρ V/s 1000/T for $Cu_{(1-x)}Zn_xFe_2O_4$ ferrites sintered at 900^OC.

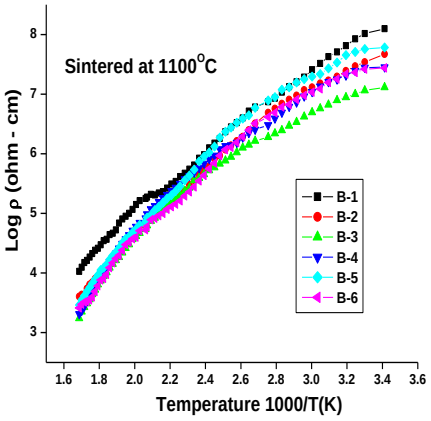

Fig. 5: Plots of Log ρ V/s 1000/T for $Cu_{(1-x)}Zn_xFe_2O_4$ ferrites sintered at 1100^OC.

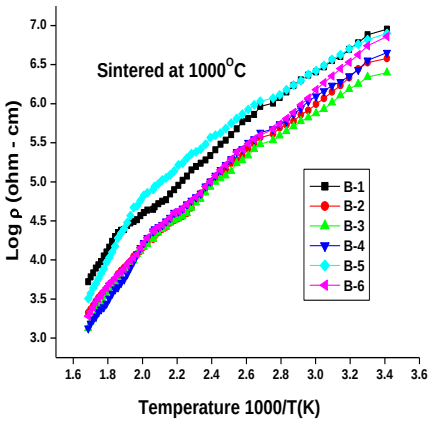

Fig. 4: Plots of Log ρ V/s 1000/T for $Cu_{(1-x)}Zn_xFe_2O_4$ ferrites sintered at 1000^OC.

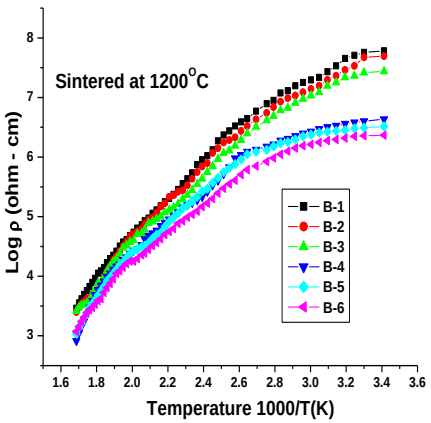

Fig. 6: Plots of Log ρ V/s 1000/T for $Cu_{(1-x)}Zn_xFe_2O_4$ ferrites sintered at 1200^OC.

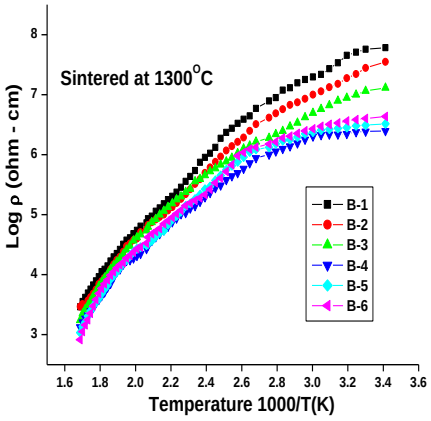

Fig. 7: Plots of Log ρ V/s 1000/T for $Cu_{(1-x)}Zn_xFe_2O_4$ ferrites sintered at 1300^{O}C.

The DC resistivity ρ for the ferrite system $Cu_{(1-x)}Zn_xFe_2O_4$ was calculated within the range of temperature 300K to 450K. The observed values of dc resistivity is in agreement with the reported for Cu-Zn spinel ferrite[21] accordingly the ferrite system under investigation over the studied range of temperature behaves as semiconducting materials. In this study we can observe the structure change from tetragonal structure to cubic structure[22] and magnetic transition from ferrimagnetic state to paramagnetic state[23]

Dielectric measurements as a function of temperature in the range 300 ~ 450 K were carried out using a LCR meter (HP-4284A model) in conjunction with a laboratory designed cell, temperature controller (± 1°C) using two probe method. The dielectric constant was calculated by using the formula

$$\varepsilon'_T = \frac{C_s t}{\epsilon_o A}$$

where C_s is capacitance of pellet, t is the thickness of pellet, A the cross-sectional area of the flat surface of the pellet and ϵ_o the constant of permittivity for free space. The variation of dielectric constant ε' of $Cu_{(1-x)}Zn_xFe_2O_4$, as a function of temperature, is shown in Fig.5.4. The observed values of ε' can be directly correlated with the resistivity values. Variation of dielectric constant with temperature for the composition x = o to 1 is shown in Figure 8. From the graph it is clear that there is a variation of dielectric constant with variation temperature. An abnormal behavior was observed earlier in Cu–Zn ferrite (Rezlescu and Rezlescu 1974). According to Rezlescu, the abnormal dielectric behaviour of some ferrites is due to a collective contribution of two types of carriers *p* and *n* to the polarization. The appearance of *p*-type carriers in the present system is due to reduction tendency of Cu^{2+} to Cu^{1+} ion, which means that in the present sample the two types of conduction exist, i.e. $Cu^{2+} \Leftrightarrow Cu^{1+}$ resulting in *p*-type conduction and $Fe^{2+} \Leftrightarrow Fe^{3+}$ in *n*-type conduction. It is well known that the local displacements of *p*-type carriers take part in the polarization in an opposite direction to that of external field. In addition, since the mobility of *p*-type carrier is lower than that of *n*-type carrier, their contribution to polarization decreases more rapidly at lower frequency. Therefore, the position of peak depends on the majority of *p*-type or *n*-type carriers in the sample.

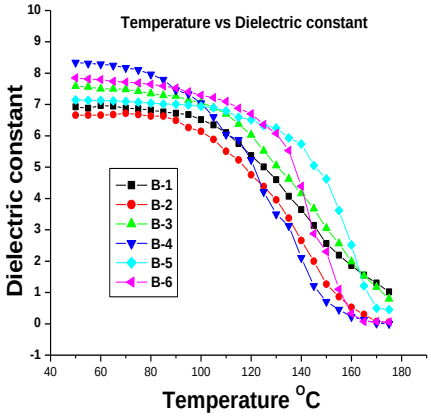

Fig. 8: Temperature v/s Dielectric Constant

In the cubic system of ferrimagnetic spinels, the magnetic order is mainly due to a super exchange interaction mechanism occurring between the metal ions in both the A and B sublattices. The substitution of non-magnetic ions such as zinc, which is having a preferential A-site occupancy results in the reduction of the exchange interaction between A and B sites. Hence, by varying the degree of zinc substitution the magnetic properties of the fine particles can be varied. Fig. 9 shows the room temperature hysteresis loop of the prepared powder samples for various zinc substitution. Upon increasing the partial substitution of zinc with manganese the specific magnetization (M_s), remanance (M_r), coercivity (H_c) and Curie temperature (T_c) decreases with increasing the zinc concentration.

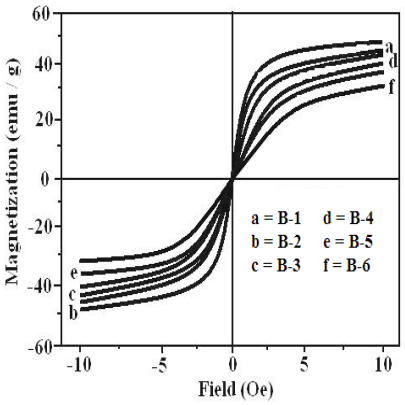

Fig. 9: Hysteresis curve of the prepared samples $Cu_{(1-x)}Zn_xFe_2O_4$.(x = 0 -1)

The variation of coercivity and remanence with increasing in the zinc substitution are shown in Fig.10. The specific magnetization measured at 10 kOe was found to be maximum (49 emu/g) for x = 0.2 and decreased on further increase in zinc concentration (33 emu/g) for x = 1. The observed changes in saturation magnetization and Curie temperature with the degree of zinc substitution are given in Fig. 11. The changes in magnetic properties such as M_s, H_c, M_r and Curie temperature T_c are due to the influence of the cationic stoichiometry and their occupancy in the specific sites. In addition, formation of dead layer on the surface, existence of random canting of particle surface spins, non-saturation effects due to random distribution of particle size, deviation from the normal cation distribution, presence of adsorbed water, etc., were due to the reduction of magnetic properties of nanosized particles.

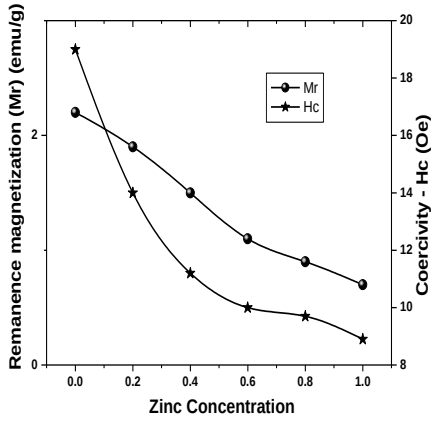

Fig. 10: Variation of coercivity and remanence with the increase in the zinc substitution

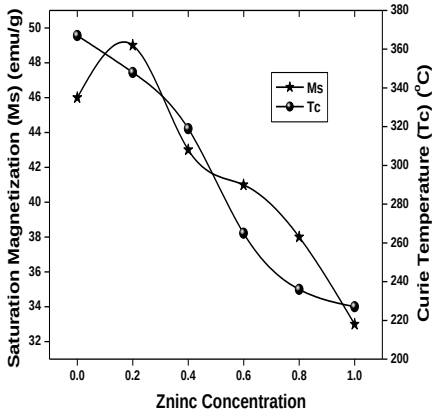

Fig. 11: Changes in the M_S and Curie temperature with the increase in the zinc substitution

Conclusion:

In the present work $Cu_{(1-x)}Zn_xFe_2O_4$ ferrite nanoparticles are prepared through co–precipitation method. The average crystallite size of the sample is in the range of 14-20 nm. The measured crystallite size values have been found to be in good agreement with the micrograph images. The saturation magnetization (M_s), remenant magnetization (M_r), and coercive force (H_c) are observed. Further investigations on the resistivity of the $Cu_{(1-x)}Zn_xFe_2O_4$ ferrite carried out by sintering of $Cu_{(1-x)}Zn_xFe_2O_4$ ferrite nanoparticles via co–precipitation method, show existence of phase transitions thus contributing to significantly to the high electrical resistivity when compared with the reported values. It is a very important parameter in minimizing the eddy current losses in power applications. It is evident that the material prepared by sintering nanomaterial Cu-Zn ferrite not only provides less loss in the material but also produces material with small grainy structure with large number of grain boundary area by inhibiting the grain growth and to suppress the phase changes. This feature showed a remarkable effect in influencing the magnetic properties in this series of samples. The semiconductor like behavior exhibited by Cu-Zn ferrite in measuring the resistivity and the values of resistivities improved than the bulk Cu-Zn ferrites.

References:

1) J.Kulikowski, J magn Matter. Vol. (41), (1984), Page (56).
2) P. Ravindranathan, K.C. Patal, Mater sci. (1997), Page (22).
3) M. Grigorova, H. J. Blythe, V. Blaskov, V.Rusaov, V.Petkov, V.Masheve, D. Nihtianova, L.M.Martinez, J.S. Munoz, M.Mikhov, J. Magn. Magn. Mater. 183, 163 (1998).
4) J. Smit, H.P.J.Wijn, Ferrites, Philips Technical Library, Eindhoven 73(1959).
5) R. Lebourgeois, J.P.Ganne and B. Lloret, J. Phys. IV France 7 Suppl. Cl: 105(1997).
6) Oliver SA, Willey RJ, Hamdeh HH, Oliveri G, Busca G (1995) Scripta Metal Mater 33(10/11):1695
7) Chen Q, Rondinone AJ, Chakoumakos BC, Zhang ZJ (1999) J Magn Magn Mater 194:1
8) Verma S, Joy PA, Khollam YB, Potdar HS, Deshpande SB (2004) Mater Lett 1092
9) Berchmans LJ, Selvan RK, Kumar PNS, Augustin CO (2004) J Magn Magn Mater 279:103
10) Basahel SN, El-Bellihi AA, Gabal M, Diefallah El-HM (1995) Thermochim Acta 256(2):339
11) Patil KC, Gajapathy D, Pai Verneker VR (1982) Mater Res Bull 17:29
12) Rupard RG, Gallagher PK (1996) Thermochim Acta 272:11
13) Li X y, Feng L B~ lm G X, et al. Preparation and characterization of nanocrystalline $ZnFe_2$ 0_4. Particles and EPR study on their properties [J]. Chemical J of Chinese Universities (in Chinese), 1995, 10:1495 – 1499
14) Wang X H, Li D, Iat L D, et al. Synthesis of substituted M-and Wtype barium ferrite nano-struclured powders by stearic acid gel method [J]. J of Alloys and Compounds, 1996, 237:45-48
15) A.GUINIER,"Radiocristallographine" (Dunod,Paris,1964)p.464.
16) Depyrot J, da Silva GJ, Alvert CR, Sousa EC, Magalha¨es M, Figueiredo Neto AM, Sousa MH, Tourinho FA (2001) Braz J Phys 31:390
17) ASTM Table No. 22–1012.
18) Evans BJ, Hafner SS (1968) J Phys Chem Solids 29:1573

19) Roy S, Ghose G (2000) J Appl Phys 87:6226
20) ASTM Table No. 25–0283
21) A.L. Eatah, A.A.Ghani and M.F.El-Shahat, Phys. State Sol.(a) Vol.(104), (1987), Page (793).
22) B.L.Patil, S.R.Sawant and S.A.Patil, Phys. State Sol. (a) (1992), Page (133-147).
23) P.V.Reddy, V.D.Raddy and D.Ravinder, Phys. State sol.(a), Vol,(127), (1991), Page (349).